Lab on a Chip

RSC Publishing

PAPER

View Article Online
View Journal | View Issue

Cite this: *Lab Chip*, 2013, **13**, 3588

Integrating biological vasculature into a multi-organ-chip microsystem†

Katharina Schimek,‡[a] Mathias Busek,‡[ab] Sven Brincker,[a] Benjamin Groth,[a] Silke Hoffmann,[a] Roland Lauster,[a] Gerd Lindner,[a] Alexandra Lorenz,[a] Ulrike Menzel,[c] Frank Sonntag,[b] Heike Walles,[d] Uwe Marx[a] and Reyk Horland*[a]

A chip-based system mimicking the transport function of the human cardiovascular system has been established at minute but standardized microsystem scale. A peristaltic on-chip micropump generates pulsatile shear stress in a widely adjustable physiological range within a microchannel circuit entirely covered on all fluid contact surfaces with human dermal microvascular endothelial cells. This microvascular transport system can be reproducibly established within four days, independently of the individual endothelial cell donor background. It interconnects two standard tissue culture compartments, each of 5 mm diameter, through microfluidic channels of 500 μm width. Further vessel branching and vessel diameter reduction down to a microvessel scale of approximately 40 μm width was realised by a two-photon laser ablation technique applied to inserts, designed for the convenient establishment of individual organ equivalents in the tissue culture compartments at a later time. The chip layout ensures physiological fluid-to-tissue ratios. Moreover, an in-depth microscopic analysis revealed the fine-tuned adjustment of endothelial cell behaviour to local shear stresses along the microvasculature of the system. Time-lapse and 3D imaging two-photon microscopy were used to visualise details of spatiotemporal adherence of the endothelial cells to the channel system and to each other. The first indicative long-term experiments revealed stable performance over two and four weeks. The potential application of this system for the future establishment of human-on-a-chip systems and basic human endothelial cell research is discussed.

Received 18th February 2013,
Accepted 7th May 2013

DOI: 10.1039/c3lc50217a

www.rsc.org/loc

Introduction

The significant impact of endothelial cell (EC) co-culture to emulate the functionality of an individual human tissue *in vitro* has been proven in various "organ-on-a-chip" systems over the last few years.[1–5] Moreover, the success in individual tissue culture microsystems has stimulated researchers to challenge a more systemic level of human biology *in vitro* through so-called "body-on-a-chip" or "human-on-a-chip" systems.[6–9] Such systems aim to combine several organ equivalents within a human-like metabolizing environment or aim at *in vivo*-like pharmacokinetics and pharmacodynamics. The most advanced of these microsystems – the micro cell culture analogue (μCCA) of Shuler and co-workers[10] – supports the molecular interplay between individual liver, bone-marrow and tumour cell culture compartments through a media recirculation using an external pump and an external common reservoir. Physiological flow velocity and substance residence times can be maintained in that system at an artificially high fluid-to-tissue ratio. The same solution for media recirculation has been used in the multi-channel 3D-micro fluid cell culture system (μFCCS) of Zhang and co-workers to combine individual human liver, lung, kidney, and adipose cell culture compartments.[11] By contrast, the total micro bioassay system of Imura and co-workers, in its most advanced version, constitutively combines human intestine, liver and breast cancer cell cultures in a single linear channel applying unidirectional flow without media recirculation.[12] The establishment of a functional on-chip organ equivalent also requires a significant period of time – *e.g.* 18 days for the most advanced lung equivalent on a chip;[1] the effective substance exposure time in most existing microsystems usually ranges from 24 to 72 h and rarely exceeds 7 days.[9] The total tissue cultivated within an individual tissue compartment rarely exceeds 10,000 cells.

[a]*Technische Universität Berlin, Institute of Biotechnology, Department Medical Biotechnology, Gustav-Meyer-Allee 25, 13355 Berlin, Germany.*
E-mail: reyk.horland@tu-berlin.de; Fax: +49-30-314-27914; Tel: +49-30-314-27913
[b]*Fraunhofer Institute for Material and Beam, Winterbergstr. 28, 01277 Dresden, Germany*
[c]*Universitätsklinikum Magdeburg, Leipziger Str. 44, 39120 Magdeburg, Germany*
[d]*Fraunhofer Institute for Interfacial Engineering, Nobelstr. 12, 70569 Stuttgart, Germany*

† Electronic supplementary information (ESI) available. See DOI: 10.1039/c3lc50217a

‡ These authors contributed equally to this work.

Therefore, the existing ''human-on-a-chip'' or individual ''organ-on-a-chip'' solutions differ from human biology in two pivotal aspects: the inability to provide unlimited tissue homeostasis, and the lack of the physiological capabilities of tissue repair. We hypothesize that a miniaturized equivalent to the human blood vasculature is a major missing part in the process of achieving such long-term homeostasis at a single individual organ or multi-organ level on chips. The human cardiovascular system is composed of two parts. The transport part – heart and vessels – ensures lifelong pulsatile blood perfusion of the capillaries in a recirculation mode. The functional part – capillaries 1–4 mm long, 5–10 μm in diameter – was designed by evolution so that maintenance (nutrition and immune defence), crosstalk (hormones and other messenger molecules) and repair (clotting and neoangiogenesis) of all organs of an individual organism is ensured. Impressive demonstrations of the power of biological vasculature for organ functionality has been provided through implantation of *in vitro* tissue cultures back into *in vivo* vasculature.[13–15]

We aimed to emulate the transport part of the human vasculature – heart and vessels – on a chip to address this gap. An on-chip micropump to support steady long-term fluid flow through a microchannel system fully covered by primary human dermal microvascular endothelial cells (HDMECs) was established. In contrast to the majority of the existing microsystems to investigate shear stress effects on ECs applying steady shear stress in the range of 10–40 dyn cm^{-2},[16–21] we aimed for pulsatile shear stress with reversing patterns which had been used earlier in different experimental settings.[22–24] The microvascular transport system presented in this work interconnects two separate compartments which are designed for the future integration of individual organ equivalents with a biomass capacity of up to 100 mg each. Special inserts were fabricated supporting vessel branching and diameter reduction in the areas of individual organ culture compartments to support later organ vascularization. Rapid prototyping applying soft lithography and replica moulding of PDMS allows the flexible adjustment of the design with regard to the number of organs and their specific arrangement, always adhering to the same standard chip basement format. Furthermore, two important features were incorporated to overcome the technical handling restraints of the majority of existing microfluidic systems: i) incubator independent operation of the microsystem was assured by a tempered chip support, and ii) microscopic access to each and every area of the circuit channels was guaranteed, enabling real-time video microscopy.

Materials and methods

Device design and fabrication

We designed and fabricated a microfluidic multi-organ-chip (MOC) device accommodating two separate microvascular circuits each operated by a separate peristaltic on-chip micropump. Fig. 1 illustrates the system. The cover-plate accommodates six air pressure fittings and four inserts forming 300 μl compartments, each for media exchange and later integration of organ equivalents (Fig. 1b). The MOC-holder supports controlled constant tempering of the MOC at 37 °C (Fig. 1a). Peristaltic on-chip micropumps (Fig. 1c) were modified from Wu and co-workers.[25] Micropump software control facilitates both clockwise and anti-clockwise fluid flow. The flow rate (Q) can be varied by the adjustment of the pumping frequency. Each microchannel circuit (Fig. 1d) comprises a total volume of 10 μl while the two individual insert-based compartments for further organ equivalent culture each have a volumetric capacity of up to 300 μl. Standard soft lithography and replica moulding of PDMS (Sylgard 184, Dow Corning, Midland, MI, USA) were been applied for MOC fabrication. In brief, a master mould was fabricated by bonding a silicon wafer to a glass wafer. Photoresist was applied to the silicon wafer and patterned by using a photomask and UV light. Subsequently unprotected silicon regions were etched and the photoresist was stripped. To fabricate the microsystem, the cover-plate (CP) was treated with a silicon rubber additive (WACKER® PRIMER G 790; Wacker Chemie, Munich, Germany) at 80 °C for 20 min. The prepared cover-plate was plugged to the master mould (channel height 100 μm, width 500 μm) and PDMS (10 : 1 v/v ratio of PDMS to curing agent) was injected into this casting station. The set-up was incubated at 80 °C for at least 60 min. Teflon screws were used to generate the four PDMS-free culture compartments and the six 500 μm thick PDMS membranes constituting the two on-chip micropumps (three membranes per micropump). The cast PDMS slice bonds fluid-tight to the CP. Thereafter, the PDMS slice attached to the CP was irreversibly bonded by low pressure plasma oxidation treatment (Femto; Diener, Ebhausen, Germany) to a microscope slide. The sterile medium was injected immediately into the two microvascular circuits to avoid surface neutralization.

Characterization of fluid dynamics

We applied non-invasive micro-particle image velocimetry (μPIV), reviewed in detail elsewhere,[26] to characterize the fluid flow in spots A and B (*cf.* Fig. 1d) of the microfluidic circuit. In brief, a Zeiss Primovert inverting microscope (Zeiss, Jena, Germany) with a standard halogen lamp as a continuous light-source, coupled to a CMOS-camera (Baumer HXC40, resolution: 2048 × 2048 pixel, interface: CameraLink; Baumer Optronic, Radeberg, Germany) was used to track the movement of 15 μm polystyrene beads (4×10^4 g ml^{-1}; Life Technologies, Darmstadt, Germany) at an exposure time of 4 μs per single image. A low magnification (4×) was chosen to constrain the shift between two frames to approximately 50 pixels (1 pixel = 3.2 μm). The z-focus was set to the centre of the fluidic channel in the respective spot (50 μm above the glass slide) to detect the peak velocity. A window at the centre of the fluidic channel (1024 pixel × 100 pixel, 3.28 mm × 0.32 mm) was observed achieving frame rates up to 3200 fps. Finally, the correlation was carried out with a software programme (Fraunhofer IWS, Dresden, Germany) which analyses an image stack of 15,000 frames, calculating the correlation maximum for the x-component of the displacement in a specified area.

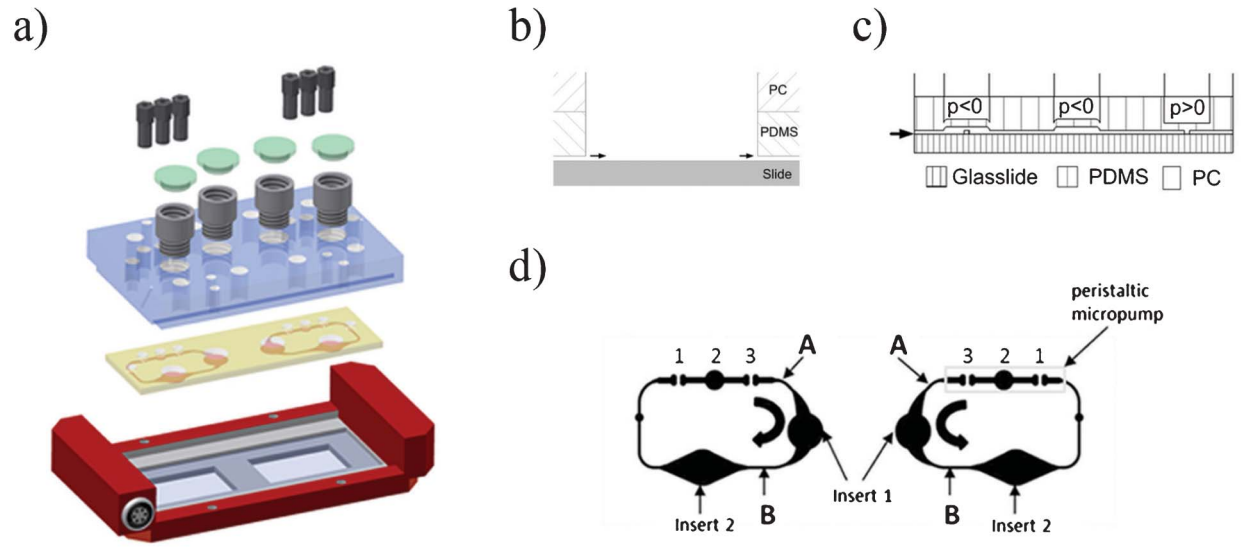

Fig. 1 The microfluidic MOC device at a glance. (a) Exploded view of the device comprising a polycarbonate CP (blue), the PDMS-glass chip accommodating two microvascular circuits (yellow; footprint: 76 mm × 25 mm; height: 3 mm) and a heatable MOC-holder (red). (b) Section through the tissue culture compartment supporting media exchange and cell/tissue cultures directly in the fluid flow. (c) Cross-section of a peristaltic on-chip micropump operated by programmed periodic compression and decompression of three successively arranged PDMS membranes (thickness: 500 μm); the arrow indicates the direction of flow. (d) Top view of the MOC layout illustrating the two separate microfluidic circuits (channel height: 100 μm; width: 500 μm) each accommodating two insert areas (compartments) (insert diameter: 5 mm). Spots A and B of each circuit designate the position of non-invasive fluid flow and cell analysis.

The calculated values of five successive frames were averaged to minimize artefacts. The following pump configuration was used for all experiments: pressure 500 mbar; vacuum −520 mbar; and air flow 1.5 l min^{-1} at 350 mbar.

The time-dependency was measured at two different places (A and B) on the chip, as shown in Fig. 1d.

The average shear stress at the channel walls with a volumetric flow of Q can be calculated by[27]

$$\tau_{cells} = \frac{6 \cdot \mu \cdot Q}{h^2 \cdot w} \quad (1)$$

for a rectangular channel (width w, height h) and the dynamic viscosity μ. The volumetric flow rate is equal to the mean flow velocity through the channel area:

$$Q = w \cdot h \cdot \bar{v} = w \cdot h \cdot k \cdot v_{max} \quad (2)$$

A calibration was carried out to determine the dependency between velocity maximum (v_{max}) and mean velocity. The fluid was pumped through the channel with a syringe pump to ensure a steady and well-defined volumetric flow rate. By varying Q, a coefficient k of 2/3 was measured.

This led to the following well-defined relationship between peak velocity and wall shear stress:[27]

$$\tau_{cells} = \frac{4 \cdot \mu \cdot v_{max}}{h} \quad (3)$$

where v_{max} is the magnitude of the averaged velocity at the centre of the channel, μ is the dynamic viscosity (calculated as 1 mPa s^{-1}) and h is the channel height (100 μm).

Cell isolation and culture

HDMECs were isolated from human foreskin obtained with informed consent and ethics approval (Ethic Committee Charité University Medicine,Berlin, Germany) from a paediatric surgery after routine circumcisions of juvenile donors. All skin samples used for cell isolation were processed within one day of their removal. Prior to isolation, the foreskins were cleaned in 80% ethanol for 30 s and rinsed with phosphate buffered saline (PBS; PAA, Coelbe, Germany). The skin-ring was opened and subcutaneous tissue was removed. In order to separate the thin epidermal layer from the dermis, the prepared foreskin was incubated in 5 mg ml^{-1} dispase II solution (Sigma-Aldrich, Schnelldorf, Germany) at 4 °C for 15–18 h. The dermis was cut into small pieces and then incubated with 4 mg ml^{-1} Collagenase NB 4 solution (Serva, Heidelberg, Germany) at 37 °C for 75 min. The mixture was passed through a 70 μm nylon filter and centrifuged at 300 g for 5 min. The resulting cell pellet was resuspended in Endothelial Cell Growth Medium MV2 (ECGM-MV2; PromoCell, Heidelberg, Germany) supplemented with Supplement-Pack MV2 (PromoCell, Heidelberg, Germany), 1% Penicillin-Streptomycin (*P*-S) and 0.05% fungizone. The cells were seeded into a T-75 flask and grown in 5% CO_2 at 37 °C. The medium was replaced one day after seeding. Two to five days after the initial seeding, the HDMECs were purified by magnetic associated cell sorting (MACS). Cells were harvested using 0.05% (0.5 mg ml^{-1}) Trypsin/EDTA (PAA, Coelbe, Germany) and a positive selection for ECs using the CD31 MicroBead Kit (Miltenyi Biotec, Bergisch Gladbach, Germany) was performed according to the manufacturer's instructions. ECGM-MV2 supplemented with Supplement-Pack MV2 and 1% P-S (complete ECGM-MV2) was used to elude the cells from

the column. A purity control of the isolated cells was performed directly after each MACS by FACS analyses. Where necessary, separation cycles were repeated until >90% of the cells were positive for CD31. The purified HDMECs were either frozen for later use or used immediately after expansion. HDMECs were expanded in T-75 flasks with complete ECGM-MV2 until 70–90% confluence at a three day feeding regimen. Cells between the 3rd and 8th passage were used for all studies to ensure that the cells retained their primary endothelial characteristics.

Culture of HDMECs on differently treated PDMS surfaces

HDMECs were seeded at a density of 10^4 cells cm^{-2} on three types of PDMS surface: untreated, coated with 100 μg ml^{-1} fibronectin (Sigma Aldrich, Schnelldorf, Germany) and treated with air plasma. Air plasma treatment was performed in a low pressure plasma system (50 W) at a frequency of 13.56 MHz for 30 s. After 48 h of cultivation, growth behaviour and morphology of the cells was compared by light microscopy.

EC seeding and culture in the MOC

Prior to seeding, each MOC was flushed with medium and incubated statically for 3 days in 5% CO_2 at 37 °C. HDMECs were harvested from expansion cultures using 0.05% Trypsin/EDTA (PAA, Coelbe, Germany). The cell suspension was concentrated by centrifugation and cell counts were performed using the ViCell viability counter (Beckman Coulter, Fullerton, CA, USA). Cell viability was >90% for all experiments. Centrifuged cells were resuspended with complete ECGM-MV2 to a final concentration of 2×10^7 cells ml^{-1}. Afterwards, the cell suspension was transferred to a 1 ml syringe. The cells were injected through one of the two compartments of each circuit. The syringe was connected to a female Luer × ¼–28 male adapter (IDEX Health & Science, Wertheim-Mondfeld, Germany). Air was pushed out of this fitting, which was then screwed to a special thread (MOC) adapter (MicCell MOC-I ¼–28 UNF × M10 Fitting (PEEK); Gesim, Dresden, Germany). An empty syringe was connected in the same way to the second compartment. After even cell infusion into both circuits the device was incubated in 5% CO_2 at 37 °C under static conditions for 3 h to allow the cells to attach to the channel walls. An amount of 300 μl fresh medium was added to each compartment and then flushed through the PDMS channels using the on-chip micropump of each circuit. A frequency of 0.476 Hz was applied to every microvascular circuit of the MOCs for continuous dynamic operation. For MOC cultures under static conditions, the channels were flushed with fresh medium for 5 min, utilising a difference in hydrostatic pressure between the inlet and outlet compartment.

An amount of 150 μl medium per compartment was replaced every 1–2 days in both dynamic and static MOC systems, and cell growth and viability were monitored by light microscopy inspection at spots A and B of each circulation (Fig. 1d). In addition, cell viability was determined with a Calcein AM assay. A solution of 5 μg ml^{-1} CellTrace™ calcein red-orange AM (Life Technologies, Darmstadt, Germany) was added into both compartments of each circuit of a MOC at a volume of 100 μl. The MOC was pumped for 2 min and then incubated under static conditions in 5% CO_2 at 37 °C for 30 min. Thereafter, the microchannels were washed twice with medium by replacing the medium in the compartment inserts with fresh medium. Images were obtained using a fluorescence microscope (BZ9000; Keyence, Neu-Isenburg, Germany). Regular MOC experiments were finished after 4 days (10 dynamic MOCs and 12 static MOCs). Individual MOCs were operated at the same mode over 7, 14 and 32 days to gain first indications of the long term performance of the microvascular circuits. In order to evaluate the possibility of replacing the CO_2-incubator for MOC operation by the MOC-holder shown in Fig. 1a, 9 MOC experiments (7 dynamic MOCs and 2 static MOCs) were performed using the holder exclusively for operation times of up to 7 days.

Characterization of EC metabolism in the MOC

The glucose concentration of the medium was measured, according to the manufacturer's instructions, using the Stanbio Glucose LiquiColor® (Oxidase) Procedure No. 1070 (Stanbio Laboratory, Boerne, TX, USA). Briefly, 99 μl of the reagent were added to a 96 microtitre plate (Greiner Bio-One, Frickenhausen, Germany) prewarmed to 37 °C and 1 μl of medium sample was added. After another 5 min of incubation at 37 °C, the glucose concentration was quantified in a microplate reader (FLUOstar Omega; BMG Labtech, Ortenberg, Germany) at 500 nm, using water as a reference.

The lactate concentration of the medium was measured, according to the manufacturer's instructions, using the LOD-PAP Method (Diaglobal, Berlin, Germany). Briefly, 99 μl of the reagent was mixed with 1 μl of medium sample in a 96-well format multiwell plate and the absorbance was measured at 520 nm in a microplate reader, using water as a reference.

Immunofluorescence staining of ECs inside the MOC

After 4 days in culture, the ECs were fixed inside the microvascular circuit with cold acetone at −20 °C for 10 min, rinsed twice with PBS for 5 min, incubated with 10% goat serum in PBS for another 20 min, and then incubated with the primary antibody, mouse anti-human CD31 (1 : 500; 7.1 mg ml^{-1}; DRFZ, Berlin, Germany), at room temperature (RT) for 2 h. Subsequently, the circuits were washed twice with PBS followed by incubation with the secondary antibody, Alexa Fluor® 594 goat anti-mouse (1 : 200, 2 mg ml^{-1}; Life Technologies, Darmstadt, Germany), in the dark at RT for 40 min. After washing, the antibody sheep anti-human vWF-FITC (1 : 50, 10 mg ml^{-1}; Abcam, Cambridge, UK) was added and incubated at RT for 2 h. Nuclei were counterstained with Hoechst 33 342 (1 : 1000, 10 mg ml^{-1}; Life Technologies, Darmstadt, Germany). Another immunofluorescence staining with the primary antibody mouse anti-human VE-Cadherin (1 : 100, 0.2 mg ml^{-1}; Santa Cruz Biotechnology, Heidelberg, Germany) was carried out: ECs were fixed with 4% PFA for 10 min, rinsed twice with PBS for 5 min and permeabilised with 0.2% Triton X-100 for 5 min. After washing twice with PBS, staining for primary and secondary antibodies was performed, as described above. MOC cultures were stained for filamentous actin with Oregon Green® 488 phalloidin (Life Technologies, Darmstadt, Germany), according to the manufacturer's instructions, in combination with VE-Cadherin.

Each solvent was added to the compartment inserts of the MOC and pumped for 1–2 min to ensure even distribution. Images were taken either by standard fluorescence microscopy or two-photon microscopy (TriMScope II; LaVision BioTec, Bielefeld, Germany). All microvascular channels were imaged through their microscope slide wall. 3D images were reconstructed from the image stack collected, using Imaris software (Bitplane, Zurich, Switzerland).

Characterization of shear stress effects

Images of immunofluorescence stained HDMECs were taken at spots A and B of each microvascular circuit (Fig. 1d) to monitor flow-induced morphological changes using a standard fluorescence microscope. HDMEC membranes on the images were retraced manually for automatic EC recognition. A connected area recognition algorithm was used to identify the ECs and calculate the corresponding perimeter, cell size, centre of gravity, and orientation (spatial unweighted second moment's main axis) of each EC. A non-dimensional shape index (SI) parameter was used to quantify cell elongation that is defined as:

$$\mathrm{SI} = \frac{4\Pi A}{P^2} \tag{4}$$

where A is the area of the cell and P is the perimeter of the cell. The SI ranges from 0 to 1, where 0 is a straight line and 1 is a perfect circle. Additionally, the angle of orientation was measured to quantify the alignment of HDMECs in the flow direction where 0° is a cell's main axis aligned perfectly with the direction of flow and 90° is a cell aligned orthogonal to the direction of flow.[28] The source code was implemented in Matlab (MathWorks, Ismaning, Germany). The SI and cell orientation angle for at least 200 cells per image were used for analysis.

Generation of microchannels structured by femtosecond laser ablation

A CAM-guided femtosecond laser (TissueSurgeon; Rowiak, Hannover, Germany) with a wavelength of 1030 nm (pulse energy = 120 nJ), a pulse duration of 400 fs and a repetition rate of 10 MHz was used by Rowiak to generate microchannels as little as 40 × 40 μm^2 into the PDMS material. The laser was focused through a microscope slide onto the surface of the PDMS-sheet with a high NA tailor-made objective lens. Channel writing was carried out by using a high-precision 3D positioning system (Feinmess, Dresden, Germany). The processing speed and laser pulse energy was set to achieve smooth and well-defined channels. We used a processing speed in the range from 50 $\mu m\ s^{-1}$ for large channels up to 5 $mm\ s^{-1}$ for small channels. The channel design was chosen to reveal minimal achievable diameters and to allow continuous media flow through each of the branched channels.

The PDMS mould was placed with its channel openings to the top into a 48-well plate to seed the pre-structured microchannels with cells. HDMECs were added on top of the PDMS mould and stained with Calcein AM assay (Life Technologies, Darmstadt, Germany) after 1 day of cultivation. Afterwards, the PDMS mould was placed with its channel openings to the bottom into the tissue compartment of the MOC, making sure that inlet and outlet channel of the pre-structured microchannel was placed in line with the channels of the MOC. Images were acquired by standard fluorescence microscopy.

Results and discussion

Evaluation of fluid dynamics

We successfully applied μPIV to characterize fluid flow profiles at different spots of the MOC circuits (Fig. 2a). Thorough microscopic access to each and every area of the MOC facilitates in-depth analyses of various other regions of the MOC and variable MOC designs in the future. Supplementary video 1 (see ESI†) illustrates the potential for optimal analysis by microscopy and the operational modus of the peristaltic micropump membranes of a microfluidic MOC circuit filled with human red blood cells from a worm's-eye view. A robust peristaltic on-chip micropump has been integrated into a microvascular circuit capable of faultlessly circulating media at sterile conditions over weeks and months at a flow rate ranging from 7 $\mu l\ min^{-1}$ (lowest frequency) to 70 $\mu l\ min^{-1}$ (highest frequency). The frequency of pulsatile operation can be increased up to 2.4 Hz, which corresponds to a high but still physiological heart activity of 144 beats per minute in humans. At this frequency, the shear stress measured at spots A and B of the microvascular circuit reaches approximately 25 $dyn\ cm^{-2}$ (Fig. 2b), which is a physiological shear stress at the higher end of the scale in microvasculature.[29] The mean velocity increased almost linearly with the pumping frequency. The pumping frequency used in our experiments (0.476 Hz) corresponds to less than 30 ''heart-beats'' per minute (approximately half of the physiological value of an adult at rest) to avoid EC loss during early phases of surface coverage. This phase somehow resembles elements of wound healing *in vivo*. As illustrated in Fig. 2a, oscillatory shear stress - another desired physiological feature - could be implemented into MOC operation through the micropump design. The waveform of such oscillation at a certain local position in the microvasculature depends upon the pumping frequency and the particular design of a MOC. Certain waveforms in humans have been associated with certain disease susceptibility.[24] This implies the further evaluation of the MOC platform for research into such pathological processes of the human cardiovascular system.

EC source, isolation and culture

Currently, the majority of human EC shear stress research in microfluidic systems is carried out on human umbilical vein endothelial cells (HUVECs) due to easy access to large cell numbers and their high phenotype pliability. We hypothesize that HDMECs own at least the same pliability of phenotype, but with a higher potential of rapid *in vitro* adaptation toward changing the local environment. Kamm and co-workers, for example, succeeded in culturing HDMECs in a vertical plane of microchannels and monitor capillary morphogenesis into collagen gels in the lateral plane.[30,31] In contrast to all other

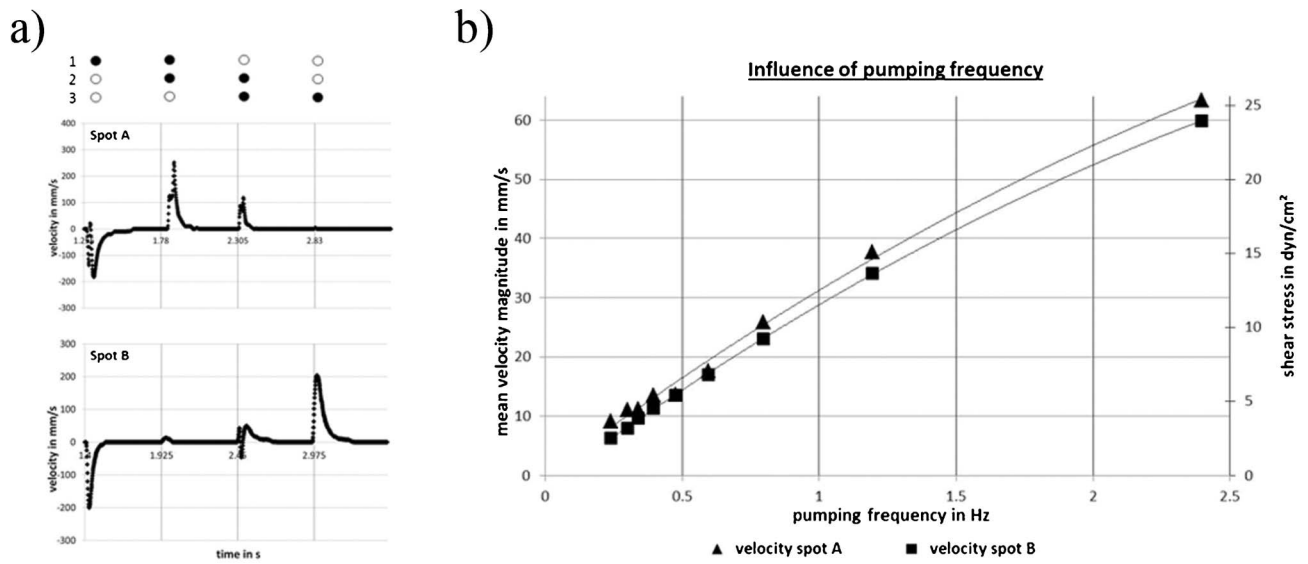

Fig. 2 Evaluation of fluid dynamics in the MOC. (a) Example of velocity profiles throughout the four stages of a full pumping cycle (frequency: 0.476 Hz) measured at the two discrete fluid flow analysis spots to underpin the pulsatile character of the fluid flow (black circle = closed valve, white circle = open valve). (b) Mean velocity magnitude (mm s^{-1}) and corresponding shear stress (dyn cm^{-2}) plotted against pumping frequencies (Hz) at both spots.

organs of the body, the skin of vertebrates needs to adapt rapidly to eventually changing external temperatures by immediate blood vessel contraction or relaxation. Moreover, the skin of carnivores is the organ with the most pronounced exposure to repeated injury, due to their aggressive life-style. These two factors taken together with human longevity might have selected HDMECs for an unmatched pliability of their phenotype and a unique potential for neoangiogenesis. Both factors are of the outmost importance for the establishment of a functional *in vitro* equivalent to human vasculature. The capacity for neoangiogenesis, in particular, is crucial for the establishment of the second part of human vasculature – the capillary network of organ equivalents – in MOCs. The latest discoveries in molecular mechanisms of angiogenesis have recently been reviewed in detail and underpin the essential role of local environment including shear stress.[32–34] Various techniques have been described to isolate human ECs from different tissues. The magnetic bead isolation of ECs after tissue digestion with CD31 (PECAM-1) MicroBeads was applied because it is constitutively expressed at the surface of virtually all types of ECs and is not present on any other cell type apart from the white blood cell population.[35,36] In particular, it is not expressed on dermal fibroblasts and smooth muscle cells. The morphology and several endothelial-specific markers were examined to confirm the endothelial origin. The isolated HDMECs showed cobblestone-like morphology in phase contrast and were positive for the endothelial-specific marker CD31, VE-Cadherin and von Willebrand Factor (vWF). Staining for 5B5, a fibroblast-specific marker, and α-smooth muscle-actin, a smooth muscle cell-specific marker, showed no outgrowth of other cell types. In addition, HDMECs showed an uptake of Alexa594-labeled ac-LDL after 4 h of exposure. A mix of dermal fibroblasts and smooth muscle cells served as the control for all stainings (data not shown). HDMECs could be cultured for up to eight passages without significant changes in morphology and marker expression. Our data indicate that this method is a robust and reproducible way to isolate CD31-positive HDMECs from human foreskin. The average number of HDMECs fully covering two microvascular circuits of a MOC was calculated to be in the range of 2×10^5 cells. On average, 1×10^7 primary HDMECs after sorting can be prepared from a single human foreskin. A cell amplification factor of ~3000 holds true between the initial seeding and passage 7–8 of HDMEC culture, thus enabling the provision of 3×10^{10} cells from a single foreskin. Theoretically, this is equivalent to 5000 cell-loaded MOCs (two circuits per MOC). Optimization of preparation and propagation might be envisioned to further improve the HDMEC yield.

Establishment of stable microvascular circuits in the MOC

A pilot comparison study between EC attachment to fibronectin-coated and air plasma-treated PDMS surfaces revealed an at least equal adherence of HDMECs to PDMS in static cultures (Fig. 3a). In addition, plasma treatment has long been recognised as a viable technique to increase the hydrophilicity of PDMS microchannels.[37–39] Therefore, air plasma treatment was finally chosen for surface activation during the fabrication of MOCs. Fibronectin is widely used as a coating material for EC attachment and cultivation in PDMS-based microfluidic devices.[28,40–42] Although easy to handle at laboratory research scale, a fibronectin coating procedure may hamper process speed and sterility at later large industrial scale at high throughput. PDMS treatment with air plasma in our hands is a reproducible, fast and scalable method to prepare PDMS-based microdevices for efficient EC attachment.

Thereafter, a microvascular circuit comprising a peristaltic micropump, two compartments for later organ equivalent cultures and connecting microchannels, entirely covered with

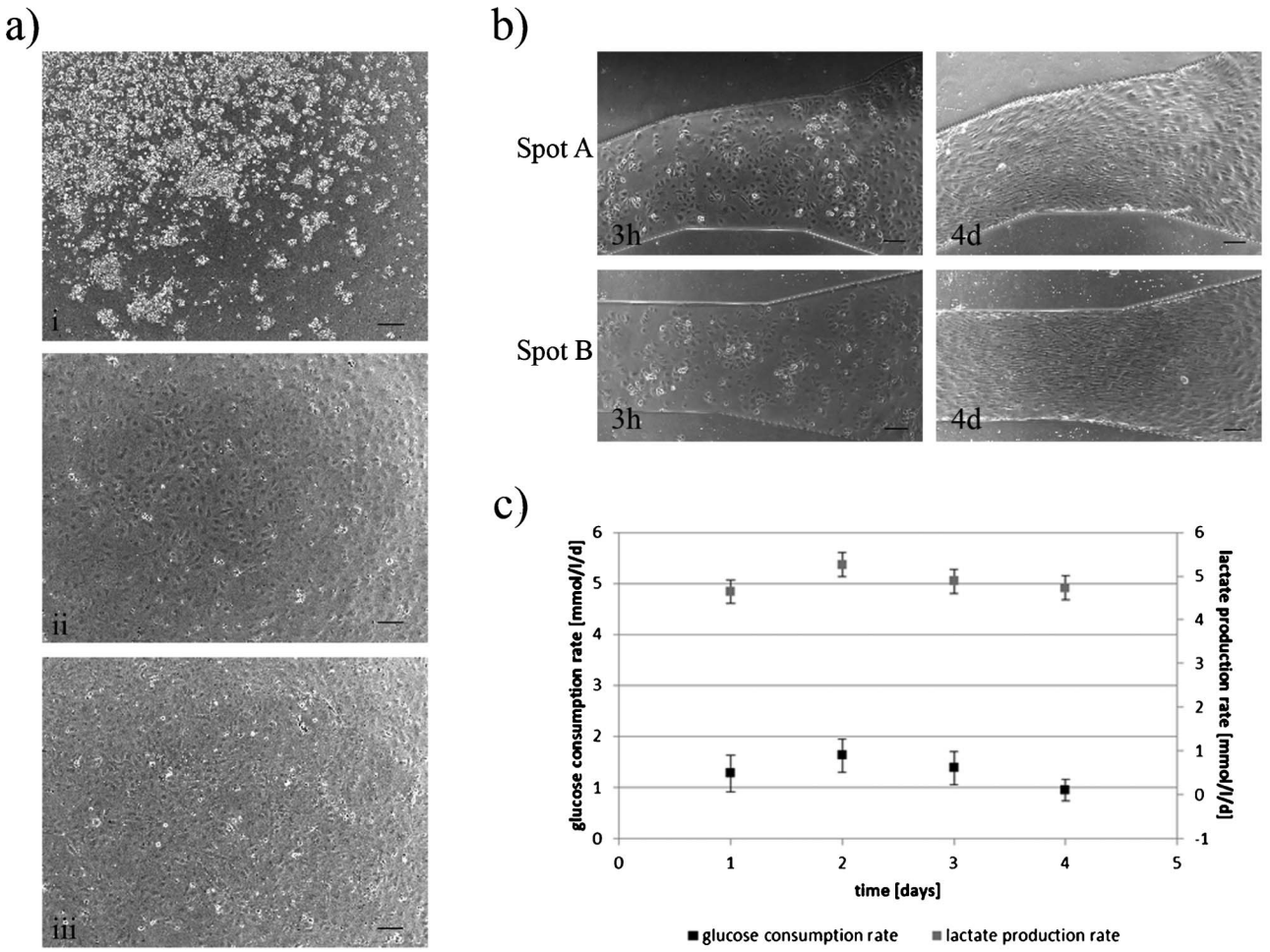

Fig. 3 Behaviour of HDMECs in the MOC device. (a) Comparison of HDMEC morphology on three different surfaces: (i) untreated, (ii) fibronectin coated and (iii) air plasma treated PDMS. Air plasma treatment supports equally pronounced adhesion of HDMECs to PDMS surfaces compared to the traditional fibronectin coating, as illustrated here for static cultures. (b) Initial cell adherence to the bottom of the channels in spots A and B observed after 3 h of static preculture differs significantly from the fully established tightly closed monolayer of the same areas after 4 days of dynamic tissue culture; a time-lapse video of the first 66 h of EC adherence to the channel bottom at spot B is provided (see ESI†, supplementary video 2). (c) The metabolic track record for glucose and lactate verifies the expected higher activity during the surface coverage (cell proliferation and attachment for ''wound healing'') until day 2 in comparison to steadily decreasing activity within a dormant ''healthy'' microvasculature (day 3 and 4). Scale bar = 100 μm.

a functional HDMEC monolayer, was established in a pulsatile media flow within 4 days of culture (Fig. 3b). We earlier demonstrated full circuit coverage with a human EC line elsewhere.[9] Here, we focussed on the rapid establishment of such a miniaturized human cardiovascular transport system based on primary HDMECs. In addition, daily tracking of the metabolic activity of ECs was performed (Fig. 3c). The increased metabolic activity within the first days of surface attachment and coverage can be explained by increased motility and proliferation of cells. Supplementary video 2 (see ESI†) visualises this increased activity in a time-lapse manner. A system attrition rate of 50% in the early stages of experiments, primarily caused by contaminations, was efficiently reduced to about 20% during routine MOC use in our laboratory. Total quality management systems installed in each and every industrial *in vitro* testing laboratory might fully eliminate this ''research lab'' attrition rate.

ECs maintained adherence to the channel walls and remained viable, as seen by Calcein red-orange AM staining. In addition, cells were tested for the uptake of Alexa594-ac-LDL (Fig. 4a). As no further change in endothelial morphology was observed after 4 days of cultivation, the experiments were stopped for analysis. In-depth immunofluorescence analyses of the tight EC layer at day 4 revealed striking viability and vascular functionality (Fig. 4a). The HDMECs forming the microvascular circuit were positive for CD31, vWF and VE-Cadherin. Furthermore, HDMECs were able to cover all walls of the channels forming a fluid-tight layer (Fig. 4b and 4c). Supplementary video 3 (see ESI†) illustrates this blood vessel-like coverage in combination with functional markers. Such stable microvascular circuits, on one hand, might act as biological membranes preventing the transfer of molecules into the surrounding PDMS slice described recently.[43,44] On the other hand, they might serve as haemocompatible vessel

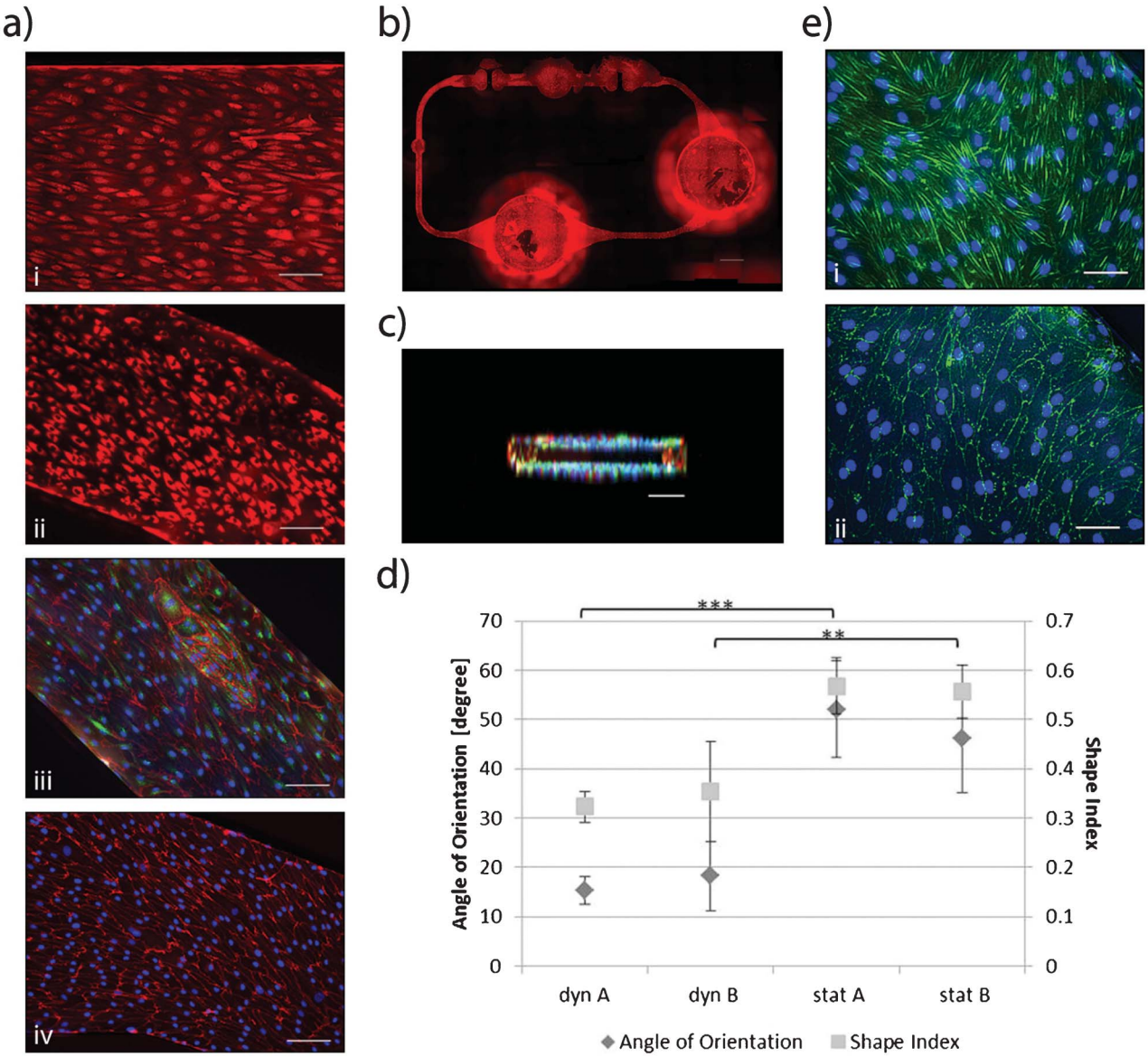

Fig. 4 Characterisation of the established HDMEC microvasculature at day 4. (a) Functionality of the established microvascular vessel system was demonstrated (as an example) for the bottom of spot A by (i) live cell viability staining (Calcein AM assay) and (ii) the uniform distribution of ac-LDL uptake, (iii) CD31 (red), vWF (green) and (iv) VE-Cadherin expression (red) throughout the entire EC population. Scale bar = 100 μm. (b) Calcein AM assay (red) showed viable and evenly distributed HDMECs in all areas of the circulation. Scale bar = 2 mm. (c) Image stack taken by two-photon laser scanning microscopy showing HDMECs inside the microchannel stained against CD31(red) and vWF (green). HDMECs were able to cover all walls of the channels forming a fluid tight layer. Scale bar = 100 μm. (d) Quantification of cell alignment (angle of orientation) and morphology (shape index, SI) of HDMECs under static and dynamic conditions at spots A and B. Comparisons between static and dynamic conditions were made by the Student t test with statistical differences established at **: $p < 0.01$; ***: $p < 0.001$. (e) Micrographs of the endothelial monolayer with fluorescently stained actin filaments in (i) dynamic and (ii) static culture conditions are shown. Bundles of stress fibres (green) align along the direction of flow in dynamically cultured ECs. Scale bar = 50 μm. Nuclei in all images were counterstained with Hoechst 33 342 (blue).

networks for whole blood circulation, preventing blood clotting.

Impact of shear stress

When exposed to laminar shear stress, ECs align themselves and their microfilaments in the direction of the flow.[45] *In vivo*, ECs in different locations are exposed to different types of flow, such as laminar, pulsatile and turbulent; the latter, for example, has been reported to increase turnover.[34] Physiological shear stress-induced elongation and flow alignment was evident in our MOC cultures plotting the SI and angle of orientation of HDMECs in the microvascular circuits generated at pulsatile flow (Q = 40.56 μl min^{-1}, τ = 5.17 dyn cm^{-2}), against those generated under static culture conditions (Fig. 4c).[46,23] A change in the distribution of filamentous actin (F-actin) was observed between static and dynamic cultivation (Fig. 4e). ECs in static conditions are polygonal and F-actin is organised as a dense band in the periphery of the cell;

meanwhile at shear stress of about 5 dyn cm^{-2}, F-actin creates bundles of stress fibres.[34] The SI and angle of orientation differed significantly between static and dynamic cultivation of ECs in the MOC (Fig. 4d), and were in the range previously reported for HDMECs in microfluidic devices.[28]

Finally, we observed equally outstanding cell viability at spots of analysis in a limited number of indicative long-term experiments with microvascular MOCs over 14 days (n = 4) of culture and in a first single microvascular MOC over 32 days (data not shown).

Preparing MOCs for vascularized multi-organ culture

It remains a formidable challenge to integrate the second functional part of the human cardiovascular system – the organ specific capillary network – into the two compartments of each microvascular MOC circuit left for future organ equivalent culture. A first successful step toward further vessel branching and vessel diameter reduction down to a microvessel scale of approximately 40 × 40 μm^2 has been accomplished applying a two-photon laser ablation technique (Fig. 5). After 1 day of static cultivation, HDMECs were distributed evenly inside the branched channels (Fig. 5a). Calcein red-orange AM staining showed viability of the seeded ECs (Fig. 5b). However, further experiments have to evaluate the potential for long-term perfused culture inside the MOC. Collagen or fibrin gels can be used to form sealed channel connections and prevent leakage during perfused culture.[47] Later on, small pores will be introduced into the PDMS mould by pre-structuring on a silanised wafer[48] or punching. Pre-cultured organoids can then be placed on top, as shown in Fig. 5a. Optical lithographic techniques have been used by Kobayashi and co-workers to perform capillary networks *in vitro* for implantation in mice.[49] Other alternatives to achieve this goal might include prevascularisation techniques,[50,51] the use of decellularised scaffolds[52–54] or tissue printing procedures involving the establishment of capillary networks.[55,56]

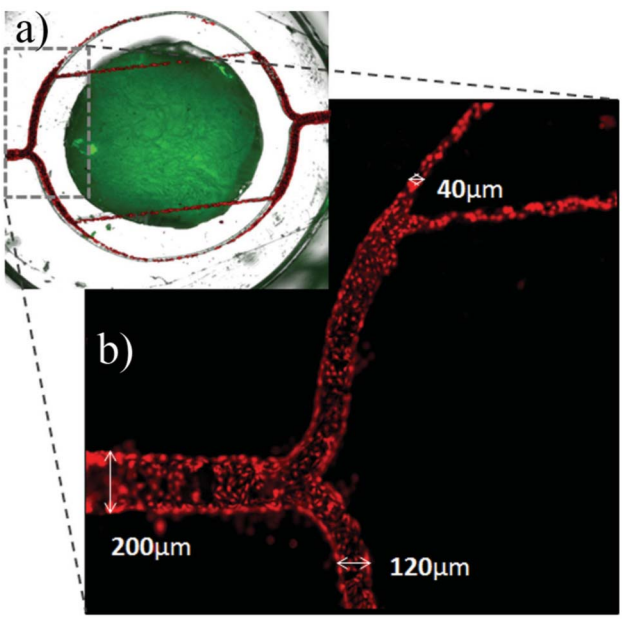

Fig. 5 Microchannels structured by Femtosecond lasers seeded with HDMECs. (a) HDMECs (red) could be distributed evenly in all branched microchannels. Green colour indicates the autofluorescence of a decellularised dermis placed exemplarily on top of the PDMS mould. (b) Calcein AM staining (red) showed excellent viability of the cells after 1 day of static cultivation.

Conclusions

Self-reliant long-term homeostasis of different organ equivalents at a miniaturized organismal scale constitutes a yet unmatched new and challenging level of *in vitro* biology in the near future. These organ equivalents need to rely on an evolutionarily optimised specialisation of each organ toward its primary function at a minute organoid level against the background of strict interdependence of all organs within an individual microsystem for survival. We hypothesize that blood circulation through EC-lined microcircuits connecting organ equivalents with each other in a physiological order is the first and prime essential requirement to fully emulate human organismal homeostasis at the microscale. Therefore, here we have successfully applied soft lithography, replica moulding and two-photon laser ablation techniques to establish an incubator independent microvascular circulation system mimicking the transport function of the human cardiovascular system at the microscale. It is arranged in a two-layer glass-PDMS chip the area of a standard microscopic slide, with channel heights of 100 μm and a total height of 3 mm. Two separate cylindrical tissue culture inserts, each the area of a standard cavity of a 96-well plate, are positioned in the microvascular circuit. A robust 4 day procedure applying pulsatile shear stress has been established to cover all fluid contact surfaces of the system with a functional, tightly closed layer of HDMECs. In contrast to the vertical plane HDMEC growth described in literature,[30,31] the entire coverage of our microvascular system with human ECs render possible biological haemocompatibility of such a microvascular system for the first time. The chip layout reduces the circulating fluid volume in the microvascular transport system down to 10 μl, at least two orders of magnitude lower than the circulation volume applied in any of the systems operated with external pumps and reservoirs. More importantly, tissue culture inserts, each of a maximum volume of 300 μl, will allow for the exact adjustment of physiological fluid-to-tissue ratios once individual organ equivalents are established in the next development step. While we could already demonstrate the successful co-culture of human skin biopsies and 3D liver spheroids over 28 days in the MOC,[57] the addition of a fully vascularized system to such a co-culture has to be implemented in the future. The fabrication technique is convenient and versatile, and design changes can be implemented in design-to-device turnaround times of only 2–3 months. The alignment and elongation of ECs in the direction of flow, thoroughly demonstrated *in vitro*,[17,18,58–60] has been monitored in perfect detail through time-lapse video microscopy. Other microfluidic channel designs have been equally efficiently covered with HDMECs in our laboratories by the technique described. We

have generated first indications that once a microvascular circulation system is established, it eventually has an operating life of at least 32 days. The unique combination of real-time video microscopy, live cell imaging and μPIV at one and the same location of the microvascular circulation system makes it a perfect tool for the basic investigation of all aspects of EC migration described,[61] such as chemotaxis, duro- or mechanotaxis,[62] haptotaxis,[63] or a combination of these cues.[64] This EC motility, as outlined by Young and co-workers, is critical to fundamental biology, pathology and tissue repair with the prime focus on understanding vasculogenic and angiogenic processes.[41]

Finally, the microvascular transport system described can now be used for the establishment of organ-specific equivalents of the functional part of the human cardiovascular system – the tissue – specific capillary network. Here, we will adhere to our recently published roadmap toward vascularised ''human-on-a-chip'' models containing a sufficient number of organs and systems to generate systemic data fully replacing the animals or human beings currently used.[9] That strategy is well in line with the concept of the Tissue Chip for Drug Screening initiative of the National Institute of Health, in collaboration with the Defense Advanced Research Projects Agency and the U.S. Food and Drug Administration launched in 2012 (http://www.ncats.nih.gov/research/reengineering/tissue-chip/tissue-chip.html).

Acknowledgements

The authors would like to thank Sebastian Schimek (Institute of Fluid Dynamics and Technical Acoustics, TU-Berlin) for invaluable help with data analysis in Matlab and Philip Saunders for the outstanding creative assistance and feedback on the manuscript. The work has been funded by the German Federal Ministry for Education and Research, GO-Bio Grant No. 0315569.

Notes and references

1 D. Huh, B. D. Matthews, A. Mammoto, M. Montoya-Zavala, H. Y. Hsin and D. E. Ingber, *Science*, 2010, **328**, 1662–8.
2 B. J. Kane, M. J. Zinner, M. L. Yarmush and M. Toner, *Anal. Chem.*, 2006, **78**, 4291–8.
3 S. R. Khetani and S. N. Bhatia, *Nat. Biotechnol.*, 2008, **26**, 120–6.
4 J. H. Sung, J. Yu, D. Luo, M. L. Shuler and J. C. March, *Lab Chip*, 2011, **11**, 389–92.
5 M. A. Guzzardi, F. Vozzi and A. D. Ahluwalia, *Tissue Eng. A*, 2009, **15**, 3635–44.
6 M. B. Esch, T. L. King and M. L. Shuler, *Annu. Rev. Biomed. Eng.*, 2011, **13**, 55–72.
7 D. Huh, G. A. Hamilton and D. E. Ingber, *Trends Cell Biol.*, 2011, **21**, 745–54.
8 H. J. Kim, D. Huh, G. Hamilton and D. E. Ingber, *Lab Chip*, 2012, **12**, 2165–74.
9 U. Marx, H. Walles, S. Hoffmann, G. Lindner, R. Horland, F. Sonntag, U. Klotzbach, D. Sakharov, A. Tonevitsky and R. Lauster, *Alternatives to laboratory animals: ATLA*, 2012, **40**, 235–57.
10 J. H. Sung, M. B. Esch, J.-M. Prot, C. J. Long, A. Smith, J. J. Hickman and M. L. Shuler, *Lab on a Chip*, 2013, **13**, 1201–1212.
11 C. Zhang, Z. Zhao, N. A. Abdul Rahim, D. van Noort and H. Yu, *Lab Chip*, 2009, **9**, 3185–92.
12 Y. Imura, Y. Asano, K. Sato and E. Yoshimura, *Anal. Sci.*, 2009, **25**, 1403–7.
13 J. D. Roh, R. Sawh-Martinez, M. P. Brennan, S. M. Jay, L. Devine, D. A. Rao, T. Yi, T. L. Mirensky, A. Nalbandian, B. Udelsman, N. Hibino, T. Shinoka, W. M. Saltzman, E. Snyder, T. R. Kyriakides, J. S. Pober and C. K. Breuer, *Proc. Natl. Acad. Sci. U. S. A.*, 2010, **107**, 4669–74.
14 J. Koffler, K. Kaufman-Francis, Y. Shandalov, S. Yulia, D. Egozi, E. Dana, D. A. Pavlov, A. P. Daria, A. Landesberg and S. Levenberg, *Proc. Natl. Acad. Sci. U. S. A.*, 2011, **108**, 14789–94.
15 W. W. Yuen, N. R. Du, C. H. Chan, E. A. Silva and D. J. Mooney, *Proc. Natl. Acad. Sci. U. S. A.*, 2010, **107**, 17933–8.
16 R. M. Nerem, M. J. Levesque and J. F. Cornhill, *J. Biomech. Eng.*, 1981, **103**, 172–6.
17 M. J. Levesque and R. M. Nerem, *J. Biomech. Eng.*, 1985, **107**, 341–347.
18 P. R. Girard and R. M. Nerem, *J. Cell. Physiol.*, 1995, **163**, 179–93.
19 S. Noria, F. Xu, S. McCue, M. Jones, A. I. Gotlieb and B. L. Langille, *Am. J. Pathol.*, 2004, **164**, 1211–23.
20 J. T. Butcher, A. M. Penrod, A. J. García and R. M. Nerem, *Arterioscler., Thromb., Vasc. Biol.*, 2004, **24**, 1429–34.
21 S. McCue, S. Noria and B. L. Langille, *Trends Cardiovasc. Med.*, 2004, **14**, 143–51.
22 G. Helmlinger, R. V. Geiger, S. Schreck and R. M. Nerem, *J. Biomech. Eng.*, 1991, **113**, 123–131.
23 J. Shao, L. Wu, J. Wu, Y. Zheng, H. Zhao, Q. Jin and J. Zhao, *Lab Chip*, 2009, **9**, 3118–25.
24 G. Dai, M. R. Kaazempur-Mofrad, S. Natarajan, Y. Zhang, S. Vaughn, B. R. Blackman, R. D. Kamm, G. García-Cardeña and M. A. Gimbrone, *Proc. Natl. Acad. Sci. U. S. A.*, 2004, **101**, 14871–6.
25 M.-H. Wu, S.-B. Huang, Z. Z. Cui and G.-B. Lee, *Biomed. Microdevices*, 2008, **10**, 309–19.
26 R. Lindken, M. Rossi, S. Grosse and J. Westerweel, *Lab Chip*, 2009, **9**, 2551–67.
27 N. Westerhof, N. Stergiopulos and M. I. M. Noble, *Snapshots of Hemodynamics: An Aid for Clinical Research and Graduate Education*, Springer, US, Boston, MA, 2010.
28 J. W. Song, W. Gu, N. Futai, K. A. Warner, J. E. Nor and S. Takayama, *Anal. Chem.*, 2005, **77**, 3993–9.
29 A. Kamiya, R. Bukhari and T. Togawa, *Bulletin of mathematical biology*, 1984, **46**, 127–37.
30 S. Chung, R. Sudo, P. J. Mack, C.-R. Wan, V. Vickerman and R. D. Kamm, *Lab Chip*, 2009, **9**, 269–75.
31 V. Vickerman, J. Blundo, S. Chung and R. D. Kamm, *Lab Chip*, 2008, **8**, 1468–1477.
32 P. Carmeliet and R. K. Jain, *Nature*, 2011, **473**, 298–307.
33 G. E. Davis, A. N. Stratman, A. Sacharidou, W. Koh and A. Sciences, *Int. Rev. Cell Mol. Biol.*, 2011, **288**, 101–165.
34 P. F. Davies, *Physiol Rev.*, 1995, **75**, 519–560.

35 J. R. van Beijnum, M. Rousch, K. Castermans, E. van der Linden and A. W. Griffioen, *Nat. Protoc.*, 2008, **3**, 1085–1091.
36 P. W. Hewett and J. C. Murray, *In Vitro Cell. Dev. Biol.: Anim.*, 1993, 823–830.
37 R. A. Lawton, C. R. Price, A. F. Runge, W. J. Doherty and S. S. Saavedra, *Colloids Surf., A*, 2005, **253**, 213–215.
38 S. Bhattacharya, A. Datta, J. M. Berg and S. Gangopadhyay, *J. Microelectromech. Syst.*, 2005, **14**, 590–597.
39 D. Bodas and C. Khan-Malek, *Sens. Actuators, B*, 2007, **123**, 368–373.
40 D. M. Spence, N. J. Torrence, M. L. Kovarik and R. S. Martin, *Analyst*, 2004, **129**, 995–1000.
41 E. W. K. Young and C. A. Simmons, *Lab Chip*, 2010, **10**, 143–60.
42 T. D'Amico Oblak, P. Root and D. M. Spence, *Anal. Chem.*, 2006, **78**, 3193–7.
43 M. W. Toepke and D. J. Beebe, *Lab Chip*, 2006, **6**, 1484–6.
44 J. D. Wang, N. J. Douville, S. Takayama and M. Elsayed, *Ann. Biomed. Eng.*, 2012, **40**, 1862–73.
45 A. B. Fisher, S. Chien, A. I. Barakat and R. M. Nerem, *Am J Physiol Lung Cell Mol Physiol*, 2001, **281**, L529–L533.
46 B. L. Gray, D. K. Lieu, S. D. Collins, R. L. Smith and A. I. Barakat, *Biomed. Microdevices*, 2002, **4**, 9–16.
47 C. Winkelmann, Y. Luo, A. Lode, M. Gelinsky, U. Marx and F. Sonntag, *Biomedizinische Technik. Biomedical engineering*, 2012, **57**, 982–985.
48 D. Huh, B. D. Matthews, A. Mammoto, M. Montoya-Zavala, H. Y. Hsin and D. E. Ingber, *Science*, 2010, **328**, 1662–8.
49 A. Kobayashi, H. Miyake, H. Hattori, R. Kuwana, Y. Hiruma, K. Nakahama, S. Ichinose, M. Ota, M. Nakamura, S. Takeda and I. Morita, *Biochem. Biophys. Res. Commun.*, 2007, **358**, 692–7.
50 L. Tian and S. C. George, *J. Cardiovasc. Transl. Res.*, 2011, **4**, 685–98.
51 I. Montano, C. Schiestl, J. Schneider and L. Pontiggia, *Tissue Eng. A*, 2010, **16**, 269–282.
52 H. Mertsching, T. Walles, M. Hofmann, J. Schanz and W. H. Knapp, *Biomaterials*, 2005, **26**, 6610–7.
53 K. Scheller, I. Dally, N. Hartmann, B. Münst, J. Braspenning and H. Walles, *Tissue Engineering: Part C*, 2013, 1–45.
54 J. Heine, A. Schmiedl, S. Cebotari, M. Karck, H. Mertsching, A. Haverich and K. Kallenbach, *Artif. Organs*, 2011, **35**, 930–40.
55 C. Norotte, F. S. Marga, L. E. Niklason and G. Forgacs, *Biomaterials*, 2009, **30**, 5910–7.
56 J. S. Miller, K. R. Stevens, M. T. Yang, B. M. Baker, D.-H. T. Nguyen, D. M. Cohen, E. Toro, A. A. Chen, P. A. Galie, X. Yu, R. Chaturvedi, S. N. Bhatia and C. S. Chen, *Nat. Mater.*, 2012, **11**, 1–7.
57 I. Wagner, E.-M. Materne, S. Brincker, U. Suessbier, C. Fraedrich, M. Busek, F. Sonntag, D. Sakharov, E. Trushkin, A. Tonevitsky, R. Lauster and U. Marx, *Lab-on-a-Chip*, 2013, DOI: 10.1039/C3LC50234A.
58 C. F. Dewey, S. R. Bussolari, M. A. Gimbrone and P. F. Davies, *J. Biomech. Eng.*, 1981, **103**, 177–185.
59 S. Noria, D. B. Cowan, A. I. Gotlieb and B. L. Langille, *Circ. Res.*, 1999, **85**, 504–514.
60 R. F. Viggers, A. R. Wechezak and L. R. Sauvage, *Journal of Biochemical Engineering*, 1986, **108**, 332–337.
61 L. Lamalice, F. Le Boeuf and J. Huot, *Circ. Res.*, 2007, **100**, 782–94.
62 S. Li, N. F. Huang and S. Hsu, *J. Cell. Biochem.*, 2005, **96**, 1110–26.
63 S. Cattaruzza and R. Perris, *Matrix Biol.*, 2005, **24**, 400–17.
64 N. Soga, N. Namba, S. McAllister, L. Cornelius, S. L. Teitelbaum, S. F. Dowdy, J. Kawamura and K. A. Hruska, *Exp. Cell Res.*, 2001, **269**, 73–87.

